ESA Cloud_cci

Algorithm Theoretical Baseline Document v5.0
FUB AATSR MERIS Cloud retrieval (FAME-C)

(Applicable to Cloud_cci version 2.0 products)

Issue 5 Revision 0

12 September 2017

Deliverable No.:	D-2.1
ESRIN/Contract No.:	4000109870/13/I-NB
Project Coordinator:	Rainer Hollmann Deutscher Wetterdienst rainer.hollmann@dwd.de
Technical Officer:	Dr. Simon Pinnock European Space Agency Simon.Pinnock@esa.int

Document Change Record

Document, Version	Date	Changes	Originator
Version 1.1	09/12/11	FAME-C ATBD draft	C. K. Carbajal Henken
Version 2.1	08/05/13	FAME-C ATBD revision, according to ESA comments. Main modifications: • Complete revision of section 2.1 (Physics of the Problem) • Correction of equations • Update of references • Formatting	R. Lindstrot + C. K. Carbajal Henken
Version 3.0	08/11/13	• Including updates/results of optional work package (WP 9081); section 2.2.3 • Updating front page of document • Minor corrections	L. Gómez Chova, M. Stengel, R. Lindstrot
Version 4.0	15/05/2015	• Including text on Bayesian cloud mask • Minor updates in text • Including several new references • Update on RTTOV version • Including a section on Pavolonis cloud typing • Added two references • Minor corrections • Editorial finalization. • Issued version.	C. K. Carbajal Henken, M. Stengel
Version_5.0 submitted version	21/04/2017	• Changing name of document • Including note on Cloud_cci version 2.0 datasets on front page • Updates: CER, CLA, text added in sections background and technical description, added figure and references etc. • Added section on OLCI stand-alone algorithm.	C. K. Carbajal Henken , M. Stengel

Table of Contents

1 Introduction

1.1 Purpose of this document

This document describes the FUB AATSR MERIS Cloud retrieval (FAME-C) (Carbajal Henken et al., 2014), which is an optimal estimation retrieval scheme for the derivation of the following cloud properties:

- Cloud Cover (CC)
- Cloud Phase (CPH)
- Cloud Optical Depth (COD)
- Cloud Effective Radius for water and ice clouds (CERwater/CERice)
- Cloud Albedo (CLA)
- Liquid/Ice water path (LWP/IWP)
- Cloud Top Temperature (CTT)
- Cloud Top Pressure (CTP)
- Cloud Top Height (CTH)

FAME-C is a synergistic daytime cloud retrieval algorithm for top-of-atmosphere (TOA) radiance measurements by MERIS and AATSR, with both instruments mounted on the polar orbiting satellite ENVISAT (and accordingly OLCI & SLSTR on the future SENTINEL-3 satellite). It uses optimal estimation to provide error estimates (and pixel quality flags) on a pixel basis (Rodgers, 2000).

1.2 Background

Clouds determine the amount of solar radiation scattered back into space and block the terrestrial radiation from the earth’s surface. An increase in globally averaged cloud-top height of 1 km results in 1.2K increase in surface temperature (Ohring and Adler, 1978). Furthermore, a 1% change in cloud cover is estimated to have more than twice the effect of a CO_2 doubling (Ramanathan *et al.*, 1989). The most important cloud properties with respect to global climate change are the cloud amount, the cloud-top height and temperature, the cloud optical depth and the size of cloud droplets. Global observations of these parameters, available from space borne instruments, are needed for the evaluation and improvement of global circulation models.

For the retrieval of COD and CER we propose a common method (Nakajima and King, 1990), whereby one channel in the visible (AATSR 0.6 micron) and one channel in the near-infrared (AATSR 1.6 micron) wavelengths are used. The principle of this method is that the cloud reflectance in the visible wavelength is primarily a function of COD, while the cloud reflectance in the near-infrared wavelength is primarily a function of particle size.

The brightness temperatures from the AATSR infrared channels (11 and 12 micron) can be used to retrieve CTT. This thermal technique, based on the strong absorption and emission of cloud layers in the thermal infrared, is typically sensitive to the uppermost part of the cloud. For thick clouds with an emissivity close to one, this brightness temperature is close to the actual cloud top temperature.

For the retrieval of cloud-top pressure we propose a method based on reflected solar radiance measured within a few nanometers of the MERIS oxygen A-band absorption centred at λ=761nm. This method was first proposed by Yamamoto and Wark (1961). Besides theoretical investigations, airborne measurements have shown that the cloud-top pressure and the cloud optical depth can be inferred from multi channel measurements of the reflected solar radiation (Wu, 1985; King, 1987; Nakajima and King, 1988; Fischer *et al.*, 1991). The approach of obtaining satellite-borne O_2 *A* band-based cloud-top pressure measurements is illustrated in Figure 1-1. The sunlight reaching the cloud-top is backscattered and a fraction finally reaches the sensor on board a satellite. For a well mixed atmospheric gas like oxygen and a known vertical profile of pressure and temperature, the traversed air mass can be estimated by radiance measurements within an absorption band. For monochromatic light in a non-scattering atmosphere, the relation between the amount of absorption and the traversed air mass can be described by Lamberts law. However, this simple approach is not sufficient because it neither includes scattering of radiation inside and outside the cloud nor correctly describes the absorption of non-monochromatic light. The impact of microphysical cloud properties, varying cloud optical depth, surface albedo as well as the observation geometry on the radiances can be investigated by radiative transfer simulations only. For the development and definition of a cloud-top pressure algorithm, the use of radiative transfer models is advantageous. With these, a systematic analysis of the influence of cloud and surface properties as well as of the influence of measurement errors can be conducted.

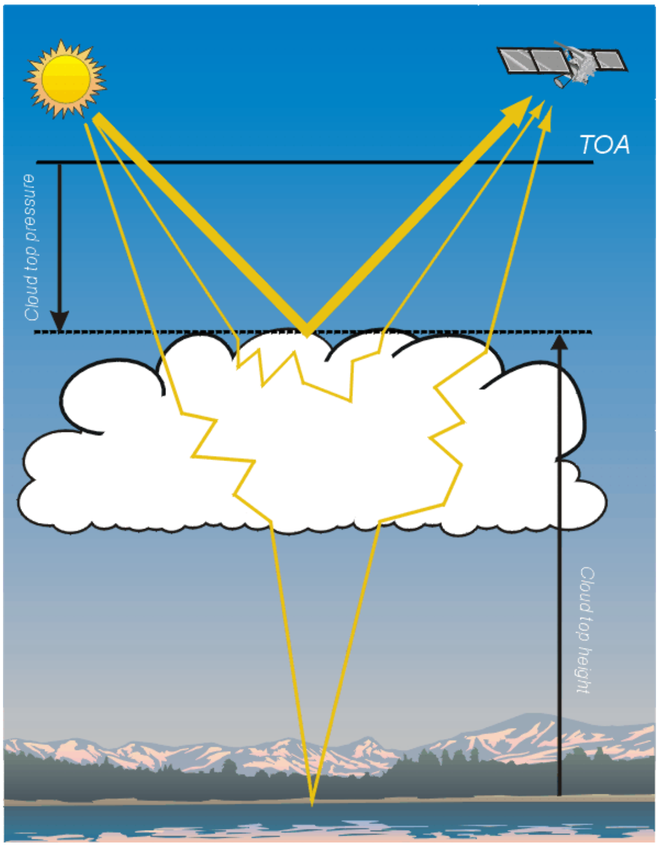

Figure 1-1 *Schematic view of various photon paths in the atmosphere. In a cloudy case, the mean photon path length depends mainly on cloud top pressure.*

1.3 MERIS and AATSR instruments

Radiance measurements from 2 bands of the Medium Resolution Imaging Spectrometer (MERIS) and radiance and brightness temperature measurements from 4 bands of the Advanced Along Track Scanning Radiometer (AATSR) are used for the retrieval of cloud macrophysical as well as optical and microphysical properties. Both instruments are mounted on the ESA polar orbiting satellite ENVISAT, which was operational from 2002 to 2012 and flies at 800 km altitude in a sun-synchronous orbit with an equator crossing time of 10.30 AM, descending node, and 98.5° inclination. Table 1-1 lists all bands for MERIS and AATSR and the ones used in the FAME-C algorithm.

MERIS has fifteen spectral bands in the solar spectral range between 390 nm and 1040 nm. The instrument scans the Earth's surface using the pushbroom method. CCD arrays provide spatial sampling in the across track direction, while the satellite's motion provides scanning in the along-track direction. The instrument has a field of view of 68.5° around nadir, shared by five identical cameras arranged in a fan shape configuration, and a swath width of 1150 km. The Earth is imaged with a spatial resolution of 1200x1000 m^2 in the reduced resolution mode. The calibration of MERIS is performed at the orbital South Pole, where the calibration diffuser is illuminated by the Sun by rotating a calibration mechanism.

AATSR has seven spectral bands in the solar, near-infrared and infrared range between 0.55 µm and 12 µm. It scans the Earth's surface with a conically scanning mirror directing radiation from two apertures onto the radiometer. This enables the instrument to view the Earth at two different angles, the nadir view and the forward view at an angle of 55° from the nadir. At nadir, the pixel resolution is approximately 1x1 km^2 with a swath width of 512 pixels. The instrument is designed to be self-calibrating. Two integrated thermally controlled black-body targets are used for calibrating the thermal channels, whereas an opal visible target is illuminated by sunlight for calibrating the visible/near-infrared channels.

The two follow-up instruments for MERIS and AATSR will be the OLCI (Ocean and Land Colour Instrument) and SLSTR (Sea and Land Surface Temperature Radiometer) on the future SENTINEL-3 satellite. This will ensure continuity in the observations.

Table 1-1 and Table 1-2 present are all MERIS and AATSR bands. Bands that are used in the FAME-C algorithm are highlighted in red.

Table 1-1 *MERIS spectral channels.*

Channel	Wavelength [nm]	Bandwidth [nm]
1	412.5	10
2	442.5	10
3	490	10
4	510	10
5	560	10
6	620	10
7	665	10
8	681.2	7.5
9	708.75	10
10	753.75	7.5
11	761.75	3.75
12	778	15
13	865	20
14	885	10
15	900	10

Table 1-2 *AATSR spectral channels*.

Channel	Wavelength [nm]	Bandwidth [nm]
1	550	20
2	665	20
3	865	20
4	1610	60
5	3740	380
6	10850	900
7	12000	1000

1.4 Algorithm Overview

The FAME-C algorithm retrieves the cloud properties in a sequential manner: first, cloud detection is performed. Then, the optical and microphysical retrieval is performed, followed by the retrievals of the cloud height products, using the output of the first inversion step as input. Prior to the main processing, a synergy product is generated using all AATSR and MERIS bands. This is done using an adapted version of a synergy tool developed at the University of Valencia (Gomez-Chova et al., 2010) and part of the BEAM software (Fomferra and Brockmann, 2005). The tool collocates the AATSR pixels on the MERIS grid. A Bayesian cloud mask method, which was developed with the help of data produced with the synergy and cloud mask tool, is used for cloud detection (Hollstein et al., 2015). and produces a Net CDF file with a band containing cloud probability. Next, an adapted version of the Pavolonis (Pavolonis et al., 2005) cloud typing algorithm is applied to the AATSR measurements to retrieve cloud type. Then, the cloud microphysical retrieval is performed for cloudy pixels to generate COD and CER daytime products. In turn, a daytime LWP/IWP product can be computed. Finally, the cloud height retrieval is performed to generate CTP and CTT products. Note that the optical and microphysical cloud properties from the previous step are used as input in the cloud height retrieval A schematic view of the algorithm is shown in Figure 1-2.

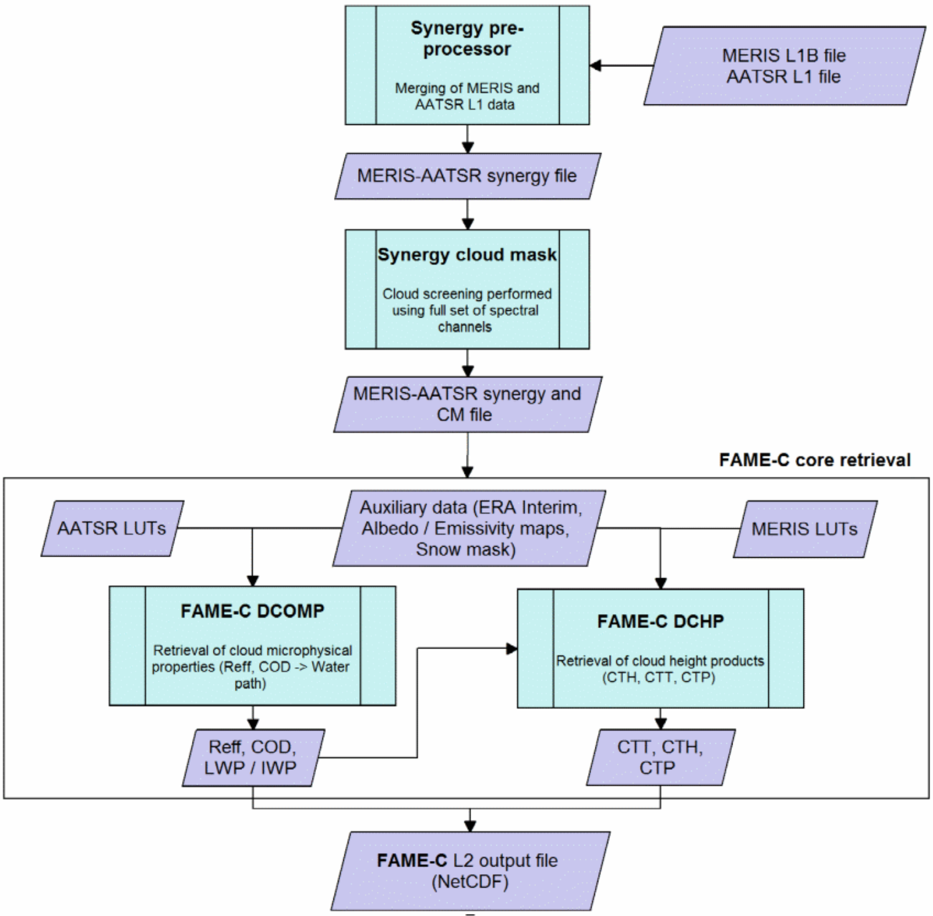

Figure 1-2 *FAME-C algorithm flow chart*

2 Algorithm description

This chapter first presents the physics of the problem, with a focus on the different techniques applied to AATSR and MERIS data for retrieving cloud height. Second, the technical description of the algorithm is given, with a short description of the radiative transfer simulations performed to produce the LUTs and the equations and error covariances used in the optimal estimation scheme within the algorithm. Third, a description is given of the three main steps within the algorithm (cloud screening, cloud optical and microphysical retrieval and cloud height retrieval), accompanied with schematic views of the cloud property retrievals.

2.1 Physics of the Problem

The retrieval of the microphysical cloud products is based on the Nakajima-King method (Nakajima and King, 1990), whereby measurements in the visible and near-infrared part of the spectrum are used to simultaneously retrieve cloud optical depth and effective radius. The underlying idea is that the cloud optical depth mainly depends on the reflectance in the absorption-free visible wavelengths, while the effective radius mainly depends on the reflectance in the near-infrared wavelengths. The cloud optical depth describes the amount of light scattered by the cloud. The effective radius describes the influence of the cloud droplet size distribution on the absorption and redirection of photons, which in turn is described by the scattering phase function. From the cloud optical depth and the effective radius, and using a number of assumptions, the amount of water in a cloud column can be computed in the form of liquid water path and ice water path, depending on the phase of the cloud.

In the second part of the algorithm, two cloud height products are retrieved which show different sensitivities to the cloud vertical profile (Lindstrot et al., 2010; Preusker & Lindstrot, 2009; Henken et al., 2013; Carbajal Henken, 2015). This difference in information from both instruments is of advantage compared to other cloud height retrievals.

The CTT retrieved from AATSR brightness temperatures is close to the actual cloud top temperature for thick clouds (emissivity near one), for which the influence of the surface is lower. Typically, the retrieved CTT is close to a cloud height where a cloud optical depth of one is reached. For optically thin clouds, the emitted surface radiation can have a large impact on the observed signal. This may result in high measured brightness temperatures for clouds which are actually located at high altitudes and are therefore much colder than measured. In contrast, the oxygen transmittance, as observed with the MERIS Oxygen-A band channel, is influenced by scattering at, within and below the cloud and therefore generally corresponds to backscattering at a level inside or below the cloud rather than to the cloud top itself (Fischer and Graßl (1991); Wang et al. (2008)). The distance between this "scattering height" and the cloud top is a function of the total cloud optical depth, the vertical distribution of cloud extinction and the surface reflectance.

Generally, the absorption of radiation within the oxygen-A band is a function of the photon path length in the atmosphere, with the ratio of radiances within and outside the absorption band providing information on the absorber mass penetrated by the photons. The appearance and the position of clouds significantly alter the possible photon path lengths. Figure 2-1 shows simulated radiances in the wavelength domain of the O_2 A-band for different cloud-top pressures. In both panels, the enhanced absorption for higher cloud-top pressures is clearly shown. For a sun zenith angle $\upsilon_S=0^\circ$ and nadir view, there is only a minor dependency of window radiances on cloud-top pressure (Figure 2-1, top panel). For higher sun zenith angles, the effects of aerosol and Rayleigh scattering increase and cause lower intensities in window channels for lower cloud-top heights (Figure 2-1, bottom panel)

The vertical profile of a cloud affects the radiances within and outside the oxygen absorption band differently. While radiances in window channels only depend on total optical thickness, radiances within the absorption band are also related to the vertical distribution of liquid water. Photons penetrating into deeper cloud layers have a higher probability of being absorbed. In Figure 2-2 the ratio of simulated radiances at λ=760nm and λ=753.75nm is shown in a polar plot and a principal plane representation. The left and right side of the figure belong to the same cloud optical properties and cloud-top pressure but they differ in geometrical thickness of the clouds (Δz=1km and 4km). The ratio of radiances at λ=760nm and λ=753.75nm is smaller for clouds with a larger geometrical thickness because the photons penetrate into deeper cloud layers.

The information on the penetration depth is required for a precise cloud-top pressure retrieval. In previous studies, the photon penetration was found to be the most challenging process to account for and to predict within the retrieval scheme (Fischer and Graßl, 1991; Fischer and Kollewe, 1994). For typical water clouds the liquid water content increases with height above the cloud base until a maximum in the upper half is reached (Pruppacher, 1980). Also, the liquid water content of different cloud types such as stratus, stratocumulus and cumulonimbus differ only by a factor of two as long as the temperature does not exceed 280K (Feigelson, 1984). According to this, the variation of liquid water content and its vertical distribution are limited.

Consequently, in a validation study the cloud-top pressure retrieved from MERIS oxygen-A band measurements was found to be highly accurate for low-level water clouds (Lindstrot et al, 2006). In contrast, a higher uncertainty is expected for clouds with a large vertical extent, due to the larger natural variability of extinction profiles and resulting photon penetration depths for these cloud types.

In summary, the combined observations of AATSR and MERIS provide complementary sensitivities with respect to cloud height:

1. Measurements in the thermal infrared spectral range allow for an accurate estimate of the cloud top temperature for optically thick clouds. In the upper atmosphere, the cloud top temperature can be converted to cloud top height / pressure with only small uncertainty, using temperature profiles from NWP data. In the lower atmosphere, this conversion is subject to larger errors, due to the somewhat uncertain emission of water vapour above the cloud and the frequent occurrence of temperature inversions.
2. Measurements of the oxygen transmittance enable highly accurate retrievals of cloud top pressure for low clouds that are characterized by a small variability of vertical extent and liquid water profile. For optically very thick clouds, the accuracy of the cloud height retrieval is lower due to the uncertainty introduced by the unknown vertical extinction profile.

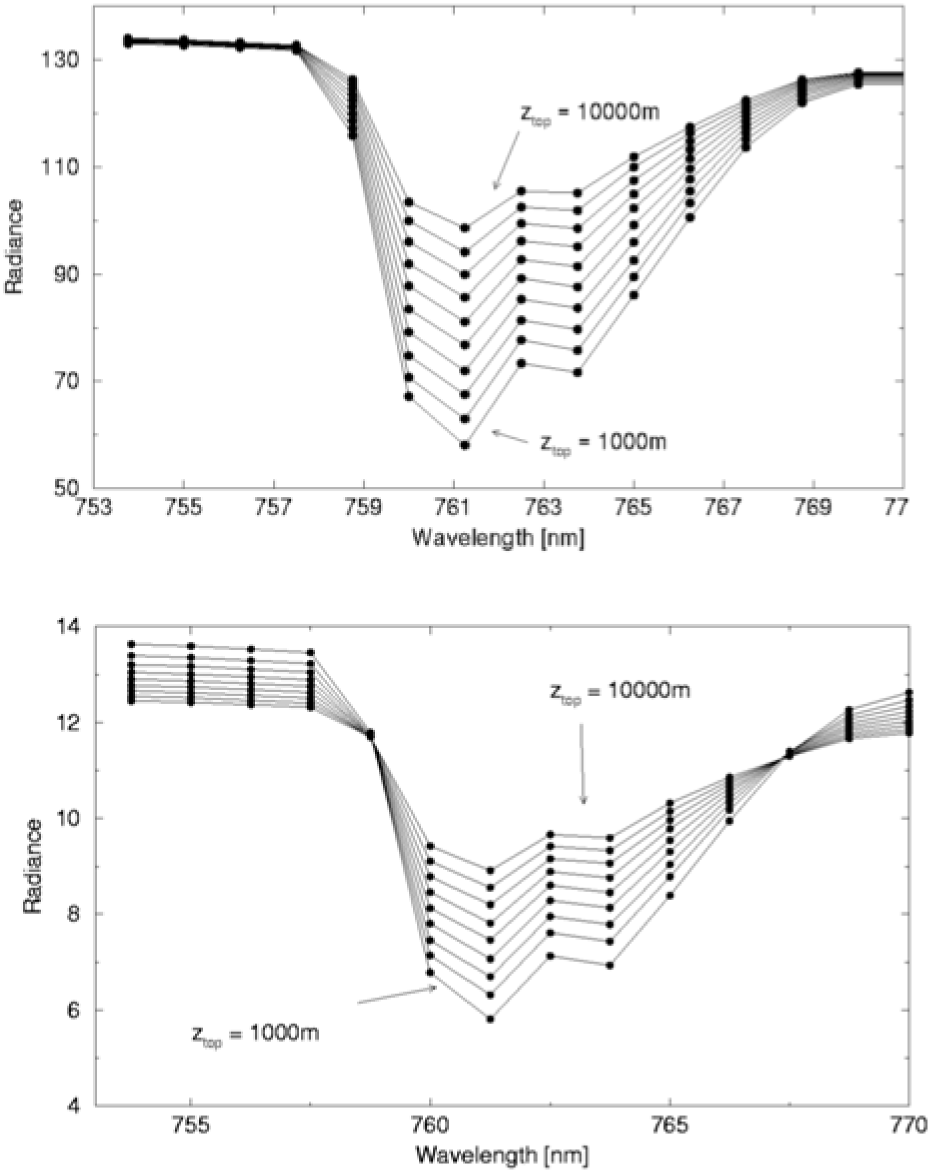

Figure 2-1 *Simulated radiances in the O2 A-band with different cloud-top pressures. Calculations for solar zenith angle □S=0° (top) and solar zenith angle □S=82.15° (bottom) and for the cloud parameters: optical thickness COD=25, geometrical thickness CGT=1000m and effective radius re=8µm. Radiance values in W / m² sr µm.*

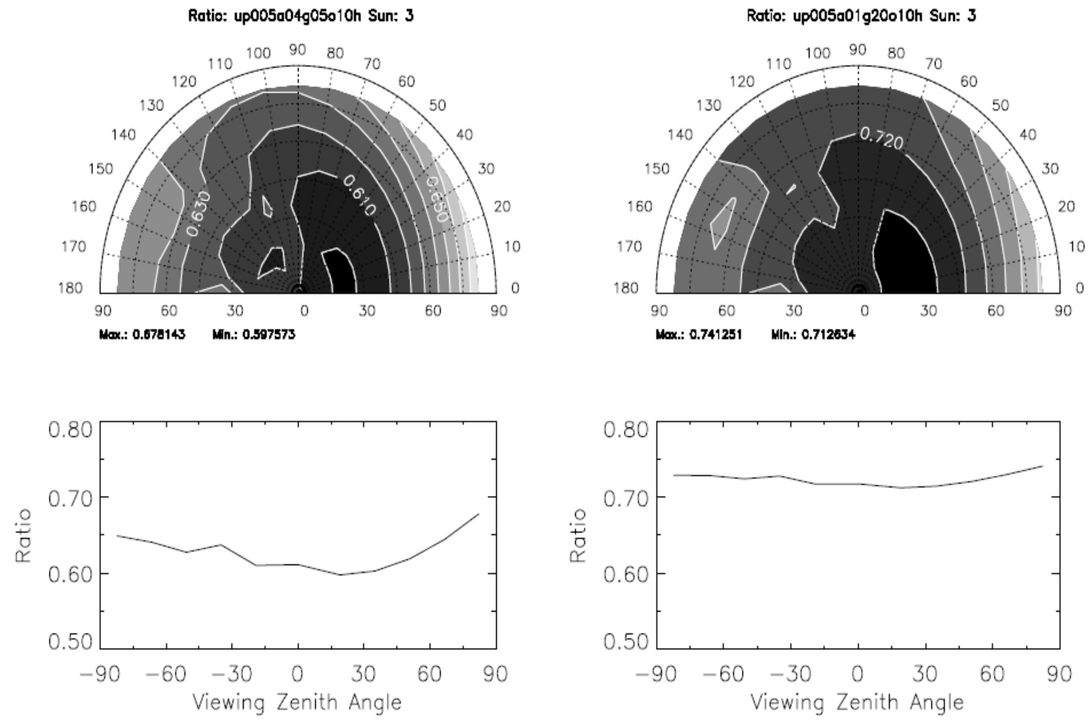

Figure 2-2 *Polar plot and principle plane graph of the simulated field of the ratio between radiances in the O_2 A-band at □ =761nm (bandwidth w=1.25 nm) and in the window channel at □=753.75nm. Calculations are done for solar zenith angle $□_S$=35° and for the cloud parameters optical thickness COD=20, cloud-top height CGT=10km, and effective radius r_e=8µm. The geometrical thickness is CGT=4km (left) and CGT=1km (right).*

2.2 Technical Description

The forward models are defined by simulating satellite radiances with a radiative transfer model (RTM) for given cloud, atmosphere and surface conditions and a specific observation geometry. The satellite radiances are stored in Look-Up-Tables (LUTs). To obtain the cloud parameters, an inverse model has to be applied to find the best fit between the simulated and observed radiances. In FAME-C this inverse problem is solved using the optimal estimation technique (Rodgers, 2000), which takes into account measurement, forward model and forward model parameter errors and a priori knowledge. For further details see Carbajal Henken et al. (2014) and Carbajal Henken (2015).

2.2.1 Radiative transfer simulations

All AATSR and MERIS Look-Up-Tables (LUTs) have been created using the radiative transfer model Matrix Operator Model (MOMO) developed at the Freie Universität Berlin (Fischer and Graßl, 1984; Fell and Fischer, 2001; Hollstein and Fischer, 2012). This code assumes a plan parallel atmosphere, however any vertical inhomogeneity and media of any optical thickness as well as any spectral resolution can be considered. In order to account for the radiation that is backscattered anisotropically from clouds, the simulations have to be performed for a wide range of observation geometries. In order to account for the required accuracy in cloud-top pressure determination, the model atmosphere is divided into 40 layers.

Since the surface reflection affects the radiance even above thick clouds, variations in surface albedo have to be taken into account. The reflection at the surface is assumed to be isotropic.

The scattering and absorption processes due to aerosols and cloud particles are represented by appropriate scattering and extinction coefficients and the corresponding scattering phase function. These parameters are obtained by Mie theory (Wiscombe, 1980) for water clouds. The influence of aerosol scattering is almost negligible in cloudy atmospheres. The simulations use a *continental* aerosol type with a constant optical thickness of AOT=0.1 at λ=550nm. Sensitivity studies have shown that the influence of varying cloud droplet size distributions *n(r)* is only of minor importance for the used cloud-top pressure retrieval algorithm (Fischer and Graßl, 1991; Preusker & Lindstrot, 2009). A modified gamma function has been adopted for the cloud droplet size distribution (Hansen, 1971). For ice clouds, the scattering properties were calculated using bulk scattering models provided by Baum et al. (2005). All cloud layers were assumed to have a cloud fraction of 1.

A correlated k-distribution method is used to incorporate gaseous absorption (Bennartz and Fischer, 2000). The approximation of transmission functions with exponential sums is used for the spectral integration within the radiative transfer code. This is necessary for the integration of the MERIS channels which are influenced by molecular absorption. The calculation of the gas absorption is based on the HITRAN 2008 dataset (Rothman *et al.*, 2009), which contains parameters of the single absorption lines of the main atmospheric gases.

The penetration depth of the photons in the MERIS Oxygen-A absorption channel is mainly determined by the cloud top pressure, but also depends on the vertical extinction profile, which in turn depends on the combination of the cloud optical depth and geometrical thickness of each cloud layer. To take into account a variety of cloud vertical extinction profiles, it was decided to derive average vertical extinction profiles for nine cloud types (Figure 2-3) using 1 year of combined CloudSat and MODIS data (Henken et al., 2012). Radiative transfer simulations for the MERIS channels have been performed using these vertical cloud profiles (Figure 2-3), which depend on cloud optical depth and cloud top pressure. The effective radius is set to fixed values for water (10 micron) and ice clouds (40 micron).

The AATSR VIS/NIR channels have been simulated without any atmosphere constituents (no gaseous absorption) and with a surface albedo of 0. Therefore, the LUTs contain top-of-cloud reflectance. The simulations distinguish different cloud types that are specified through the effective radius and ranges of cloud optical depth. Simulations have been performed using water and ice scattering phase functions and assuming homogeneous vertical cloud profiles.

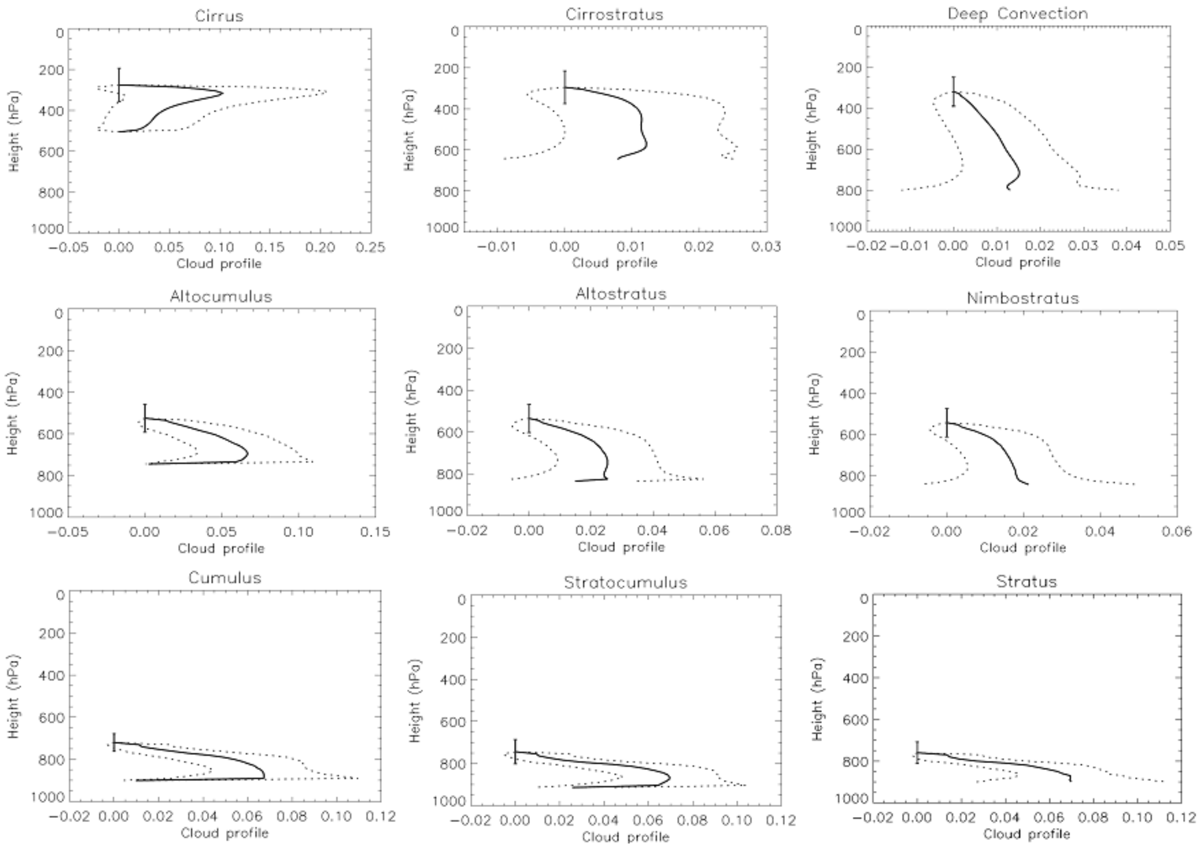

Figure 2-3 *Average cloud vertical extinction profiles for nine cloud types (solid line) and standard deviation from the mean (dotted line), as well as standard deviation of the cloud top pressure (error bar on top).*

2.2.2 Optimal Estimation Scheme

The optimal estimation technique maximizes the probability of the retrieved state, given by the values in the state vector **x**, conditional on the measurement (measurement vector **y)** and the given a priori knowledge (a priori state vector $\mathbf{x_a}$). It is assumed that the errors in the measurements (errors of forward model **F**(**x**) included) and a priori parameters show a Gaussian distribution. Accompanying covariances are given by $\mathbf{S_y}$ and $\mathbf{S_a}$, respectively. The solution for the state vector is found by minimizing the cost function J, given by

$$J(\mathbf{x}) = (\mathbf{F(x)} - \mathbf{y})^T\, \mathbf{S}^{-1}_\mathbf{y}\, (\mathbf{F(x)} - \mathbf{y}) + (\mathbf{x} - \mathbf{x_a})^T\, \mathbf{S}^{-1}_\mathbf{a}\, (\mathbf{x} - \mathbf{x_a})$$

This minimization is done in an iterative manner using the Levenberg-Marquardt method, whereby the gradient is used to find an estimate of the state which is predicted to have a lower cost. The gradient is represented by the Jacobian matrix **K** with elements,

$K_{ij} = \delta y_i / \delta x_j,$

representing the partial derivatives of the forward model with respect to each state vector parameter. K is calculated by linearizing the forward model (interpolation within the LUTs). To initiate the minimization procedure, a first guess of the state has to be given at the start of the iteration. The minimization procedure continues until convergence is achieved or the maximum number of iterations is reached (here imax = 10). Convergence is achieved when the cost function has a value below a defined threshold. Retrievals that do not show convergence within the maximum allowed number of iterations are considered to be invalid. The solution covariance is given by:

$$\mathbf{S_x} = (\mathbf{S}^{-1}_{\mathbf{a}} + \mathbf{K}^T\mathbf{S}^{-1}_{\mathbf{y}}\mathbf{K})^{-1}$$

2.2.3 Pre-processing: synergy product, cloud screening and cloud typing

From the standard L1b products of AATSR and MERIS a new product is created which contains a direct copy of all components of the MERIS L1b file (master product), i.e. band data, tie-point grids, flag codings, bitmask definitions, and metadata. The components of the AATSR L1b file (slave product) are transferred in a different manner: The non-overlapping areas of the master and slave products are cropped. The band data of the slave product are then re-sampled to match the geographical raster of the master product. For the MERIS/AATSR collocation, a nearest-neighbour re-sampling is applied. For flag bands and bands for which a valid-pixel expression is defined, the nearest neighbour method is also used. In order to establish a mapping between the samples in the master and the slave rasters, the geographical position of a master sample is used to find the corresponding sample in the slave raster. If there is no sample for a requested geographical position, the master sample is set to the no-data value, which was defined for the slave band. The collocation algorithm requires accurate geo-positioning information for both master and slave products. As for the master product, the tie-point grids, flag codings and bitmask definitions of the slave product are copied. Slave product metadata are not transferred.

Once a collocated MERIS-AATSR product is generated with the Synergy pre-processor, the cloud screening can be applied. The cloud mask is the main product of the cloud screening module. It is obtained by combining a set of neural networks that have been optimized for MERIS and AATSR synergy products under different situations. The cloud index is also computed by an artificial neural network and is included as an additional band in the synergy product. In particular, cloud detection is considered as a two-class (binary) classification problem. In order to obtain the final classifier, one has to decide: (1) which features are fed into the classifier; (2) which training samples are used to select model parameters; (3) which is the most appropriate machine learning algorithm; and (4) how to combine the individual decisions of the set of trained classifiers in order to obtain the optimal ensemble of classifiers for our particular problem. We review all these crucial steps in the following subsections.

Input Features: The proposed method exploits the combined information of MERIS and AATSR instruments, such as the high spectral and radiometric resolutions of MERIS, the oxygen absorption feature on MERIS (proxy of surface pressure), the water vapour absorptions, and shortwave-infrared (SWIR) and thermal (TIR) information from AATSR. Together with the spectral features, spatial features are extracted at different scales: the mean and standard deviation are computed for each pixel-based feature at two different scales in 3x3 and 5x5 windows.

Labelled Training Set: To obtain training samples with a true label ('cloudy' or 'cloud-free') is not an easy task since coincident simultaneous cloud data are not available for MERIS and AATSR at the same resolution. Consequently, many situations covering a wide range of real scenarios were simulated using coupled surface and atmospheric RTMs in order to use them for developing the supervised cloud classifiers. The advantage of this approach is that it provides a set of at-sensor radiance spectra with known atmospheric and surface conditions. That way, the methodology can be used to determine the presence or absence of clouds, which is specified by the cloud optical thickness (COT) used in the RTM. However, models relying only on simulated data can provide poor results when applied to real data depending on the quality and representativeness of the simulated information used. Probably more important is the fact that they cannot take into account the data properties in the spatial domain. Therefore, the simulated samples were complemented with real AATSR-MERIS spectra labelled as cloud-contaminated or cloud-free samples in order to be used in the training of the models.

Multilayer Perceptron ANN: The multilayer perceptron (MLP) is a feed-forward artificial neural network successfully applied to supervised cloud detection. MLP is constituted by a set of interconnected neurons, which are organized in layers where the input signals (or patterns) are propagated from input nodes to output nodes. In this work, MLP is trained using the Levenberg-Marquardt algorithm, which is more efficient in terms of computational cost than the standard back-propagation algorithm. In all the cases, the neurons of the hidden layer present the hyperbolic tangent sigmoid activation function while the neuron of the output layer presents a linear output function. This facilitates the analysis of the distribution of the output values and to directly combine the outputs of several ANN in the proposed ensemble method.

Ensemble of Classifiers: The basic idea of ensemble methods is to construct a set of classifiers and then to combine their individual decisions (by means a weighted average) with the aim of providing a more accurate classifier. An ensemble of ANN outputs, which takes into account our particular problems, is used:

- *Different input features* - AATSR achieves the dual-look by rotating a scan mirror through a cone-angle with the two extreme viewing angles at nadir and forward. Results may eventually deteriorate due to temporal differences and miss-registration between nadir and forward views. In these cases, combining only MERIS and AATSR nadir views is recommended. Also, independent models are trained for the pixel-based simulations and for the real observations with spatial features.
- *Different training sets* - Differences of reflectance over land and ocean produce significant differences on the extracted features. As a consequence, splitting image pixels into two different classification problems improves the results and speeds up the process.

Moreover, the ensemble outputs can be used to provide an uncertainty estimate per sample. A low variance of the ensemble of ANNs indicates high confidence on the accuracy of the output, while an average output activation distant from the decision boundary indicates high confidence on the class assignment. Therefore, the coefficient of variation of the ensemble outputs, σ/μ, is selected to estimate the uncertainty for each detection.

For computational efficiency considerations a Bayesian cloud mask method was developed (Hollstein et al., 2014), which uses results from the Synergy cloud mask as a source of artificial truth data. Hence, the Bayesian cloud mask has as a first aim to reproduce the Synergy cloud mask. Next to the advantage of the fact that large amounts of data can be processed more efficiently, is also that the output is a probability, allowing flexibility in the choice of a probability threshold in order to get a binary cloud mask. Furthermore, this approach allows for cloud masking also in case of missing data in one or several AATSR and/or MERIS bands by using a second set of features which does not include the particular band with missing data.

Within the FAME-C algorithm, separate LUTs are used for water and ice clouds. The cloud phase detection is also performed before the FAME-C algorithm (optical and micro-physical and macro-physical retrievals) is applied to the measurements. For this, an adapted version from DWD, which in turn is an adapted version of the well-established Pavolonis cloud typing algorithm (Pavolonis and Heidinger, 2004; Pavolonis et al., 2005), is applied to the AATSR measurements for cloudy pixels only (cloud probability > 50 %). Several cloud types are defined such as water clouds, thick ice clouds, cirrus clouds, supercooled clouds, overlap clouds and fog. Cloud types for which the upper cloud layers consist of water droplets, are categorized as water clouds, while cloud types for which the upper cloud layer consists of ice crystals, are categorized as ice clouds.

2.2.4 FAME-C DCOMP: cloud optical and microphysical retrieval

The FAME-C microphysical retrieval is based on the DCOMP algorithm (Walther et al, 2010). It produces a COD/CER pair from which LWP or IWP is computed. The retrieval needs the following products from other retrievals or otherwise corresponding estimates: cloud mask, cloud top pressure and cloud phase.

Each observed pixel is assumed to consist of cloud and cloud-free layers. Atmospheric corrections are executed for the cloud-free layers above and below the cloud. For the upper layer the atmosphere is corrected for by estimating the real top-of-cloud reflectance by adjusting the AATSR-TOA measurements. To account for atmospheric absorption in the layers below the cloud a virtual surface albedo that includes the atmospheric extinction for the atmosphere below the cloud is estimated.

The result of the inversion is a COD/CER pair from which the liquid water path or ice water path will be calculated, respectively. During the COD/CER retrieval, the corresponding spectral CLAs, one for the 0.66 μm channel and one for the 1.6 μm channel, are obtained as well since they are part of the forward model. Those products, their uncertainties and a common quality flag are stored in the output arrays.

Figure 2-4 shows a schematic view of the inversion through an optimal estimation technique. Within the retrieval loop, an iterative 1D-var optimal estimation technique is applied. It starts with the definition of a priori values of the state vector and the appropriate observation covariance matrix and the a priori matrix describing the prior knowledge of the atmospheric state. The cost will be calculated for each iteration step. The cost parameter, updated at each iteration, is initialized with the largest possible value for these data. Each iteration step of the retrieval loop requires search events in the LUTs. Comparison of the TOC reflectance (the observation vector), derived from the LUTs representing the forward model, to the measurement, corrected for atmospheric absorption in the cloud free layers, defines a cost surface function. The OE algorithm's task is to find the minimum value on this surface. The gradient of the cost serves as a compass pointing downhill to the lowest cost. The a priori values can be seen as a weighting function for the cost surface and help to reduce the number of iterations needed for the algorithm to converge. If the cost falls below a pre-defined threshold, the solution is found and the retrieval loop terminates. Otherwise, if a maximal number of iterations is exceeded, no solution can be found. The quality flag gets a corresponding value.

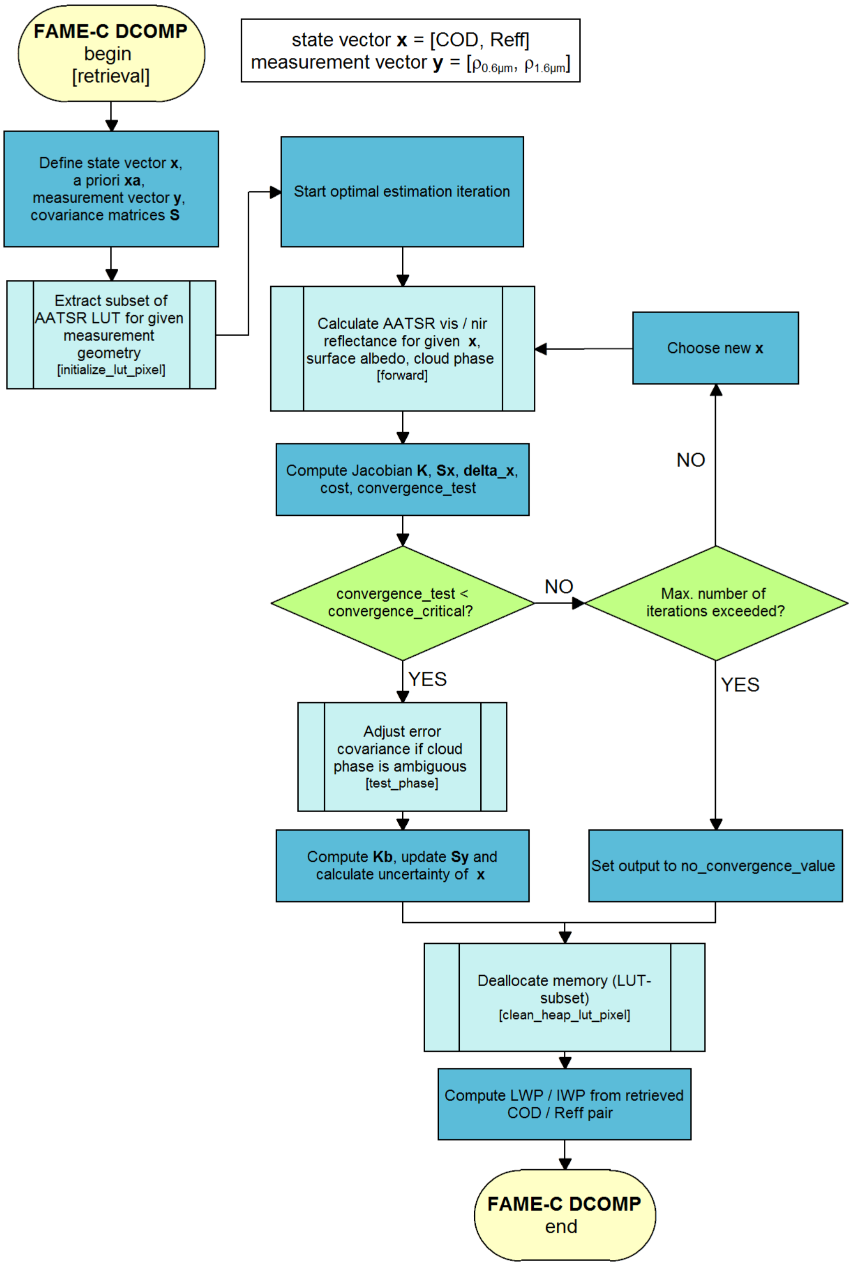

Figure 2-4 *Optimal estimation retrieval loop flow chart for FAME-C cloud microphysics retrieval.*

2.2.5 FAME-C DCHP: cloud height retrieval

The FAME-C cloud height retrieval produces two cloud height products (CTP and CTT) from MERIS and AATSR bands. It uses the MERIS radiances of bands 10 and 11 for the CTP retrieval and AATSR brightness temperatures at 11µm and 12µm for the CTT retrieval. Furthermore, auxiliary data are needed: navigation and observation geometry data, cloud mask, NWP data, surface albedo and surface emissivity, and the MERIS detector index. The latter provides information about the central wavelength of the MERIS bands. Figure 2-5 shows a schematic view of the two inversions through optical estimation technique, similarly structured as shown in Figure 2-4.

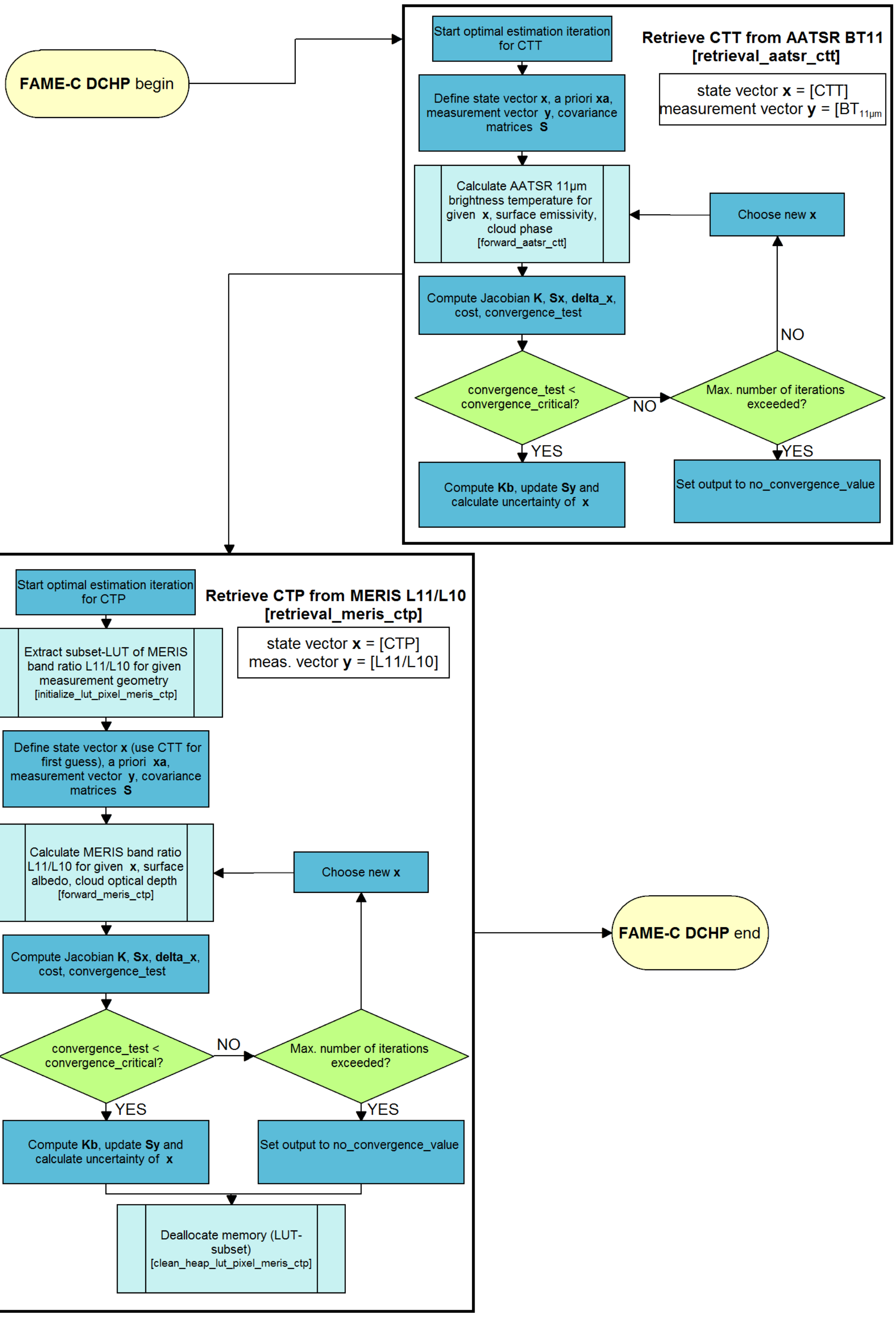

Figure 2-5 *Optimal estimation retrieval loop flow chart for FAME-C DCHP retrieval.*

3 Input and output files

This chapter lists all input files needed and all output files produced in the FAME-C algorithm.

3.1 MERIS and AATSR measurements

6 Bands from synergistic AATSR-MERIS DIMAP file (Table 1-1Table 1-2) produced using the synergistic (collocation), a probability cloud mask, as well as navigation and observation geometry data, binary cloud mask, and MERIS detector index (due to change in central wavelength of the Oxygen-A absorption band).

3.2 Look-Up-Tables

Both the AATSR and MERIS Look-Up-Tables (LUTs) have been created using the radiative transfer model Matrix Operator Model (MOMO) developed at the Freie Universität Berlin (Fischer and Graßl, 1984; Fell and Fischer, 2001; Hollstein and Fischer, 2012)

3.2.1 AATSR cloud microphysics

For the AATSR cloud microphysical retrieval there are two different kinds of look-up-tables needed. The cloud LUTs include reflection, transmittance, cloud albedo and cloud spherical albedo tables. The ancillary data LUTs include coefficients to estimate transmission in cloud-free layers for ozone and water vapour. The cloud LUTs have been created for both water and ice clouds.

3.2.1 MERIS cloud top pressure

One LUT is created assuming ice cloud particles for the upper cloud layers and water cloud particles for the lower cloud layers (depending on temperature thresholds). Based on analysis of 1 year of CloudSat-MODIS data of cloud layer optical depth and cloud geometrical thickness, average vertical extinction profiles for nine cloud types have been created and used in the radiative transfer simulations. The nine cloud types are based on COD and CTP. LUT dimensions are: CTP, COD, surface albedo, surface pressure, viewing geometry, CWVL.

3.3 Auxiliary Data

All used NWP atmospheric profiles are taken from ERA interim reanalysis data.

3.3.1 AATSR cloud microphysics

The following auxiliary data are needed:

- MODIS surface albedo maps for 0.6 and 1.6 micron channels
- MODIS snow/ice cover maps
- NWP humidity profile
- NWP total column ozone

The humidity profile and total column ozone are used to estimate the above and below cloud atmospheric absorption in the AATSR 0.6 and 1.6 micron channels. Using pre-calculated coefficients for both channels an estimate about the transmission in the cloud-free layers is made. The measured reflectance as well as the surface albedo are than adjusted for. The snow/ice cover maps are used to correct the surface albedo accordingly.

3.3.2 AATSR cloud top temperature

The following auxiliary data are needed:

- NWP atmospheric profiles for: humidity, temperature, height, ozone
- NWP surface variables: skin temperature, humidity, wind speeds, land/sea, sea ice
- MODIS surface emissivity maps
- MODIS snow/ice cover maps

The NWP data as well as the surface data are used as input for RTTOV11, which is used for clear-sky simulations. The snow/ice cover maps are used to correct the surface emissivity accordingly.

3.3.3 MERIS cloud top pressure

The following auxiliary data are needed:

- MERIS surface albedo maps
- MERIS elevation height map
- MODIS snow/ice cover maps
- MERIS stray light and spectral smile correction coefficients (NetCDF format)

The white-sky albedo map from the ESA GlobAlbedo project will be used as input for surface albedo in FAME-C for land pixels. For ocean pixels a fixed surface albedo is taken. The snow/ice cover maps are used to correct the surface albedo accordingly. With the pixel-based elevation height the surface pressure is estimated using the barometric equation.

Instrumental stray light is caused by multiple scattering and reflection at optical elements within the spectrometer like lenses or gratings. The correction of stray light is particularly important in absorption bands because weak intensities are affected strongly even by small offsets caused by stray radiation. Therefore, the O_2 *A*-band based algorithm for the retrieval of cloud-top pressure from MERIS is susceptible to errors caused by instrumental stray light. Although there is a correction for stray radiation in the operational MERIS processing chain (MERIS ground segment, Merheim-Kealy et al., 1999), artifacts are particularly apparent in pressure retrievals, which are likely to be caused by residual stray light. The quantification of the stray light effect on the retrieval errors is complicated by a high correlation with the effect of the spectral calibration uncertainty: a spectral shift of the oxygen A-band channel toward weaker or stronger absorption causes a signal similar to an under- or overestimation of the stray light contribution to the measured radiance. Because the MERIS swath is composed of the measurements of five identical cameras with individual characteristics, the errors induced by stray light and spectral calibration issues become evident particularly at the borders of the field of view of the cameras, resulting in discontinuities of the derived pressure. In order to assess the residual stray light amounts in MERIS band 11, the coefficients of a simple, brightness- and viewing angle-dependent stray light model were optimized by adjusting the derived surface and cloud-top pressure to reference data. Along with the stray light correction model, the central wavelength of MERIS band 11 was determined, both of which were found by minimizing the deviation of the derived pressure values from the truth. The effect of the residual stray light is corrected by subtracting a fraction f of the window radiance at 753nm from the radiance in the absorption channel at 761nm. Figure 3-1 shows an exemplary cloud-top pressure retrieval before and after applying the empirical stray light correction factors. Further details on the empirical stray light correction can be found in Lindstrot et al. (2010).

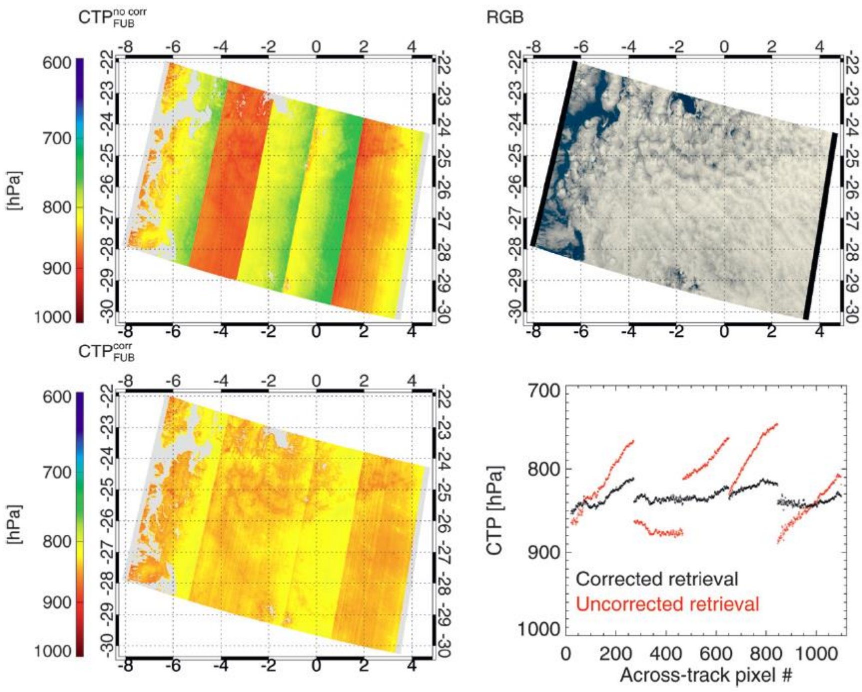

Figure 3-1 *Derived cloud-top pressure before and after stray light correction (left panels) for homogeneous, marine Stratocumulus scene. Along-track median values for complete scene are shown in lower right panel for both retrievals.*

3.4 Cloud products

The following cloud products are generated on a pixel basis:

- Cloud Cover (CC)
- Cloud Phase (CPH)
- Cloud Optical Depth (COD)
- Cloud Effective Radius for water and ice clouds (CER_{water}/CER_{ice})
- Cloud Albedo (CLA)
- Liquid/Ice water path (LWP/IWP)
- Cloud Top Temperature (CTT)
- Cloud Top Pressure (CTP)
- Cloud Top Height (CTH)

The LWP is computed from the visible COD and CER_{water} using:

$$LWP = 2/3 * COD * CER_{water} * \rho_l$$

where ρ_l is the density of water (1000 kg/m3).

For thick ice clouds the same parameterization is used, but with a slightly different factor. For thin ice clouds a parameterization proposed by Heymsfield et al. (2003) is used:

$$IWP = t_{ice}[g0(1+g1/g0)\ \ 1/CER_{ice}\ ]^{-1}$$

where t_{ice} is the visible optical thickness of the ice cloud, CER_{ice} is the effective radius in micron, and with g0 = 0.01256 and g1 = 0.725, two empirical constants.

The cloud products are accompanied by uncertainty estimates as well as quality flags based on diagnostics such as retrieval cost. Also flags indicating snow/ice cover, sun-glint, coastal pixels etc. are included.

4 Validation

4.1 A-train: MODIS, AMSR, CPR, and CALIOP

Measurements from satellite instruments which are part of the A-train are used for a statistical comparison of level 2 cloud microphysical properties as well as level 2 cloud height products. The following A-train cloud products are used for comparison:

- MODIS cloud optical depth
- AMSR LWP
- CloudSat & Calipso cloud top height

The active instruments on CloudSat (CPR) and Calipso (CALIOP) can also give information on the vertical extension of the clouds. Note that comparisons can only be made at high latitudes. Therefore, the comparison is complicated due to snow covered surfaces, sea-ice, and large solar zenith angles. Furthermore, parallax correction has to be applied for higher clouds. Also, different viewing geometries between ENVISAT and A-train instruments and time differences between overflights complicate comparisons as well. Figure 4-1Figure 4-4 show examples of validation efforts performed during the development of the FAME-C algorithm.

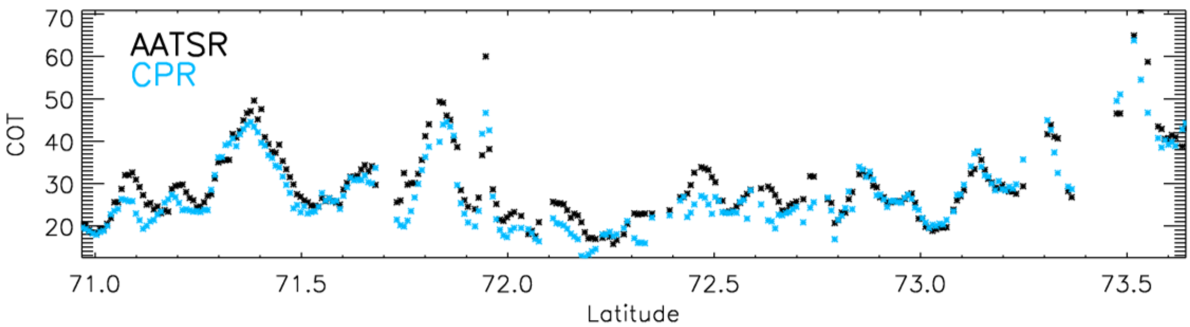

Figure 4-1 *Comparison of AATSR-COD and COD as provided in the CloudSat data, which is based on MODIS measurements, for an A-train and ENVISAT matching overflight on 3 August 2008.*

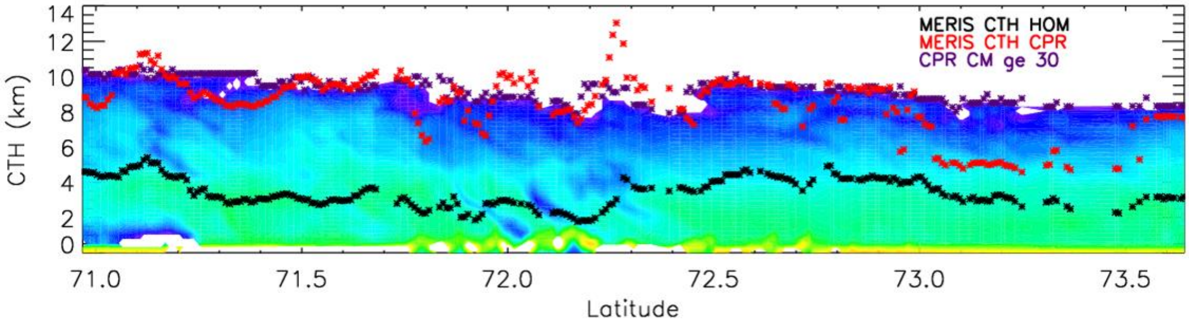

Figure 4-2 *Comparison of MERIS-CTH, assuming vertical homogenous cloud profiles (HOM) and using the nine CloudSat vertical cloud profiles (CPR), with radar reflectivity factor measurements (contours) for an A-train and ENVISAT matching overflight on 3 August 2008.*

4.2 POLIS flight campaign

During the summer of 2004 the POLIS flight campaign took place in Germany. A Portable Lidar System (POLIS) onboard of a Cessna was used to make measurements of low level water clouds during daytime. The maximum flight altitude was 3000 m. These measurements are used for validation of MERIS-CTP and AATSR-CTT. Figure 4-3 shows one of the flight tracks. The MERIS-CTP and AATSR-CTT are converted to cloud top height using radiosonde profiles for comparison against the LIDAR measurements. For low level water clouds MERIS-CTP shows an overall better performance than AATSR-CTT.

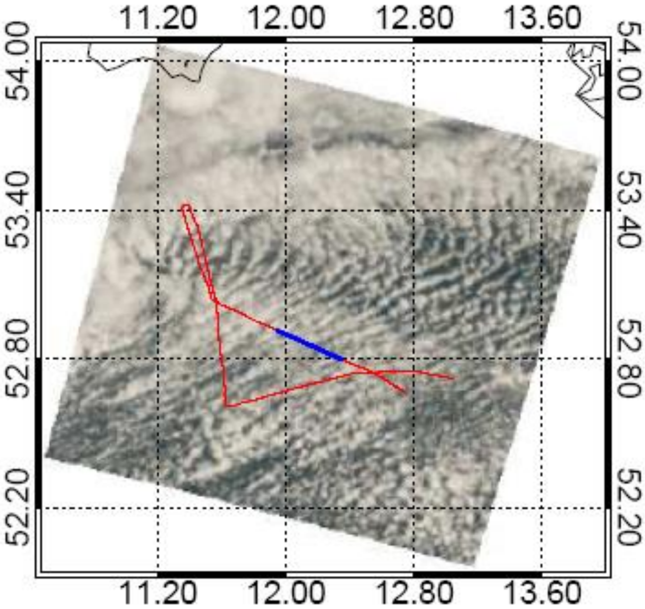

Figure 4-3 *Flight track (in red) of the Cessna on 6 June 2004. The blue section indicates the time of the ENVISAT overpass.*

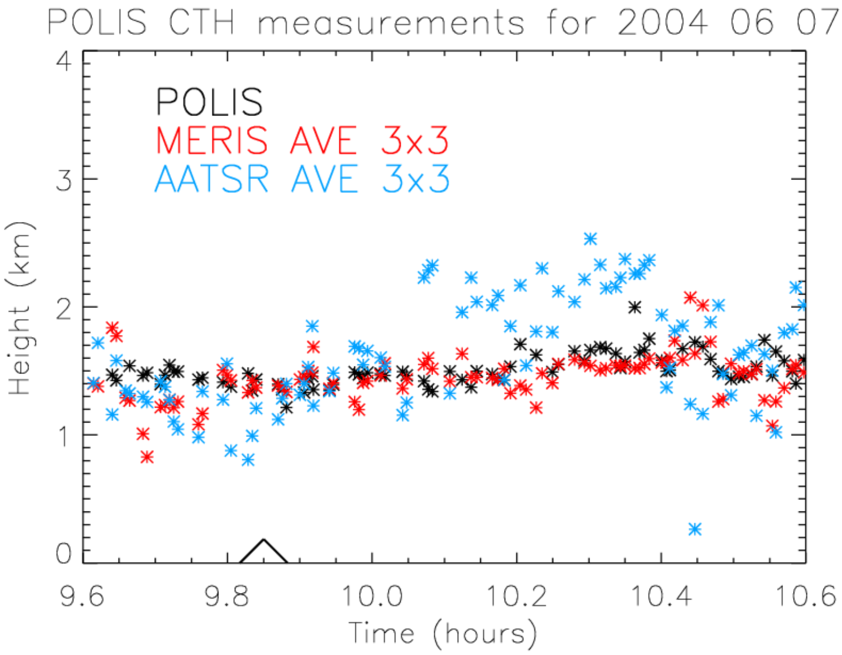

Figure 4-4 *Comparison of POLIS CTH with MERIS and AATSR retrieved CTH along the track. The MERIS and AATSR CTHs have been averaged using 3 by 3 pixels. The triangle below shows the ENVISAT overpass time.*

5 OLCI stand-alone algorithm

The Ocean and Land Colour Instrument (OLCI) is the successor of MERIS and is on board the polar-orbiting satellite Sentinel-3, which was launched in February 2016 (Donlon et al, 2012). OLCI has a slightly larger swath width than MERIS of 1270 km and a spatial resolution at nadir of about 300 m in the full resolution mode and about 1.2 km in the reduced resolution mode. Just as for MERIS, OLCI is optimised to monitor land surfaces, ocean colour over open oceans and coastal zones. Based on the excellent experience of the previous chosen MERIS channels, the MERIS channels have been kept. Importantly for atmospheric property retrievals, two additional bands, at 400 nm and 1020 nm, to improve atmospheric and aerosol correction capabilities, one additional band at 940 nm to better retrieve total column water vapour above dark surfaces have been added to the OLCI instrument. Of particular interest for cloud property retrievals are the two additional channels in the O2 A-band for improving cloud top pressure retrievals. The latter two new channels, combined with the MERIS-like channels at 753 and 761 nm, and an additional window channel at 778.75, are used in the newly developed OLCI stand-alone algorithm as indicated by the red rows in Table 5-1.

Table 5-1 *OLCI spectral channels. . Bands that are used in the OLCI stand-alone algorithm are highlighted in red.*

Channel	Wavelength [nm]	Bandwidth [nm]
1	400	15
2	412.5	10
3	442.5	10
4	490	10
5	510	10
6	560	10
7	620	10
8	665	10
9	673.75	7.5
10	681.25	7.5
11	708.75	10
12	753.75	7.5
13	761.25	2.5
14	764.375	3.75
15	767,5	2.5
16	778.75	15
17	865	20
18	885	10
19	900	10
20	940	20
21	1020	40

Equivalent to the MERIS-CTP retrieval in the FAME-C algorithm, the optimal estimation framework is used to retrieve here COT, CTP and additional information on the cloud vertical profiles, giving rise to 4 elements in the state vector **x**. Also, MOMO simulations were performed to create LUTs, which serve as forward model, and the same type of auxiliary data is needed. In the OLCI stand-alone retrieval, the measurement vector **y** consists of 5 elements. Measurements at 753.75 nm and 778.75 nm are introduced to estimate the impact of spectral surface albedo, while the absolute value at 753.75 provides information on the cloud optical thickness. The 3 bands in the O2a absorption band allow for an improved retrieval of the cloud top pressure and provide an opportunity to retrieve additional information on cloud vertical profile. The latter is expressed, next to CTP, in terms of 2 parameters: cloud geometrical thickness (CGT), or extent, and centre of gravity (CoG) or mode. As shown in Figure 5-1, extent is defined from CTP relative to the surface (range 0-1), while mode describes the height of the maximum extinction assuming a triangular form for the vertical extinction profile, ranging from CTP to cloud bottom (0-1). For now, no cloud detection is done before the cloud property retrieval. Cloudy pixels are identified in the post-processing using a minimum threshold for the COT of 0.6.

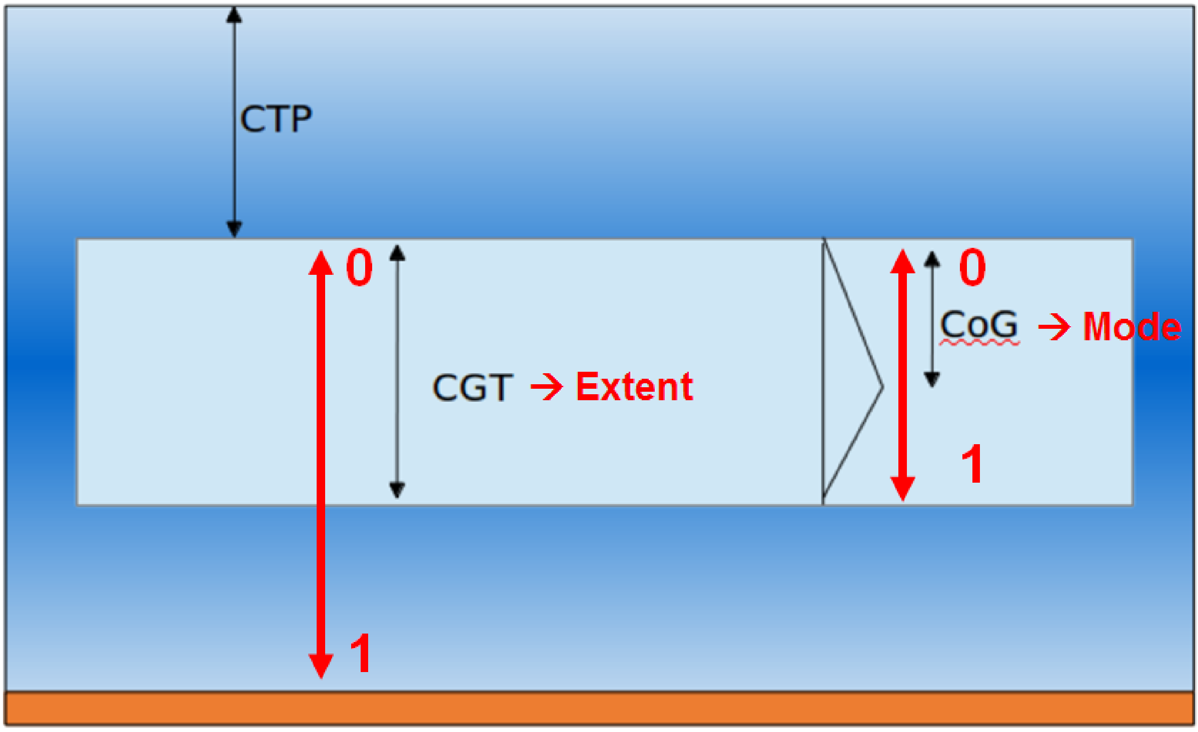

Figure 5-1 *Schematic view of the 3 retrieved parameters describing the cloud vertical structure: CTP, CGT or Extent, CoG or Mode.*

For the first processing round of two months, November and December 2016, of OLCI data in the reduced resolution mode, the a-priori mode value was given a small uncertainty, effectively meaning that the mode was more or less fixed despite being part of the state vector **x**. This was done to study the result and effect of the cloud extent first. An example scene is presented in Figure 5-2, showing high COTs and low CTPs for optically thick and high clouds and low COTs for optically thin clouds, which can be observed in the RGB image. The Extent does not show a very large variability ranging from a fraction of 0.3 to 0.7 of the atmospheric column below CTP. As expected, no variability in the mode is observed.

Extented sensivitiy studies as well as evaluation using other satellite instruments will have to give insight into the performance of the retrieval in the near future as well as to point towards cloudy situations in which it is most likely to retrieve additional information on cloud vertical profiles.

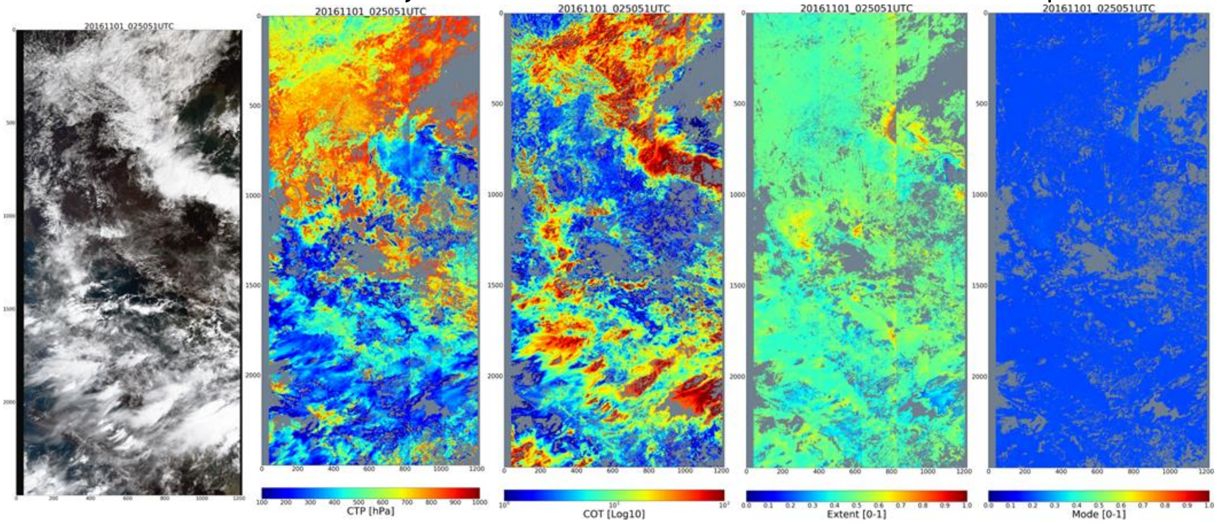

Figure 5-2 *OLCI scene for 1 November 2016 showing RGB composite and the retrieval results for CTP, COT, extent and mode.*

6 Conclusions

This document outlines the FAME-C algorithm which produces daytime level 2 cloud products from synergistic AATSR-MERIS measurements. The following cloud products are produced: cloud cover, cloud phase, cloud optical depth, effective radius, spectral cloud albedo, liquid water path/ice water path, 2 cloud top temperatures, 2 cloud top pressures, and 2 cloud top heights.

In the pre-processing synergistic AATSR-MERIS files are produced by collocating the AATSR data with MERIS data. Furthermore, a synergistic cloud mask is produced, from which cloud cover is determined. Moreover, ad adapted version of the well-established Pavolonis cloud typing algorithm is used for cloud phase detection. The first step in the main FAME-C algorithm is the daytime optical and microphysical retrieval (DCOMP) using visible and near-infrared AATSR channels. The second step is the retrieval of the two daytime cloud height products (DCHP) using AATSR infrared channels and MERIS Oxygen-A absorption channel. The cloud products are retrieved for the years 2003-20011.

The use of the synergy of the AATSR and MERIS measurements in this retrieval is advantageous over single instrument retrievals. The MERIS instrument only has channels in the visible, which means that no retrieval of the cloud microphysics can be made. This also leads to higher uncertainties in the cloud top pressure retrieval. Having both infrared channels (AATSR) and the Oxygen-A band channel (MERIS) means that two cloud height products can be retrieved, which have different sensitivities to different cloud types (Carbajal Henken et al., 2015)

Evaluation of the level-2 cloud products are performed using measurements by satellite instruments of the, e.g., A-train, flight measurements, and of ground-based observations. Also, evaluation of level-2b (daily composites) and level-3 (monthly averages) are performed using MODIS level-3 cloud products. A first version of the OLCI stand-alone cloud property retrieval is developed, aiming for the retrieval of additional information on cloud vertical structure using 3 bands in the O2a absorption band.

7 References

Baum, B. A., P. Yang, A. J. Heymsfield, S. Platnick, M. D. King, Y.-X. Hu, and S. T. Bedka, 2005b: Bulk scattering models for the remote sensing of ice clouds. Part 2: Narrowband models. J. Appl. Meteor., **44**, 1896–1911.

Bennartz, R. and J. Fischer, 2000: A modified k-distribution approach applied to narrow band water vapour and oxygen absorption estimates in the near infrared. J. Quant. Spectrosc. Radiat. Transfer, **66**, 539–553.

Carbajal Henken, C. K., R. Lindstrot, R. Preusker, and J. Fischer, 2014: FAME-C: cloud property retrieval using synergistic AATSR and MERIS observations. Atmos. Meas. Tech., 7, 3873–3890, 2014

Carbajal Henken, C. K., L. Doppler, R. Lindstrot, R. Preusker, J. Fischer, 2014: Exploiting the sensitivity of two satellite cloud height retrievals to cloud vertical distribution. Atmos. Meas. Tech., 8, 3419-3431, 2015

Carbajal Henken, C. K. Satellite cloud property retrievals for climate studies using synergistic AATSR and MERIS measurements. Dissertation Freie Universität Berlin, 2015.

Donlon, C., B. Berruti, A. Buongiorno, M.-H. Ferreira, P. Femenias, J. Frerick, P. Goryl, U. Klein, H. Laur, C. Mavrocordator, J. Nieke, H. Rebhan, B. Seitz, J. Stroede, R. Sciarra, 2012: The Global Monitoring for Environment and Security (GMES) Sentinel-3 mission. Remote Sens. of Environ., 120, 37-57

Feigelson, E. M., 1984: Radiation in a cloudy atmosphere, D. Riedel Publishing Company, Dordrecht

Fell, F., and J. Fischer, 2001: Numerical simulation of the light field in the atmosphere–ocean systemusing thematrix-operator method. J. Quant. Spectrosc. Radiat. Transfer, **3**, 351–388

Fischer, J., and H. Grassl, 1984: Radiative transfer in an atmosphere–ocean system: An azimuthally dependent matrix-operator approach. Appl. Opt., **23**, 1032–1039.

Fischer, J., and H. Graßl 1991: Detection of Cloud-Top Height from Backscattered Radiances within the Oxygen A-Band - Part 1: Theoretical Study.- *J. Appl Met.*, **30**, 1245-1259

Fischer, J., W. Cordes, A. Schmitz-Peiffer, W. Renger and P. Mörl, 1991: Detection of Cloud-Top Height from Backscattered Radiances within the Oxygen A-Band Part 2: Measurements. *J. Appl Met.*, **30**, 1260-1267.

Fischer, J. and M. Kollewe, 1994: Study of cloud top height determination using a coarse spatial resolution imaging spectrometer.- Final Report, ESA-ESTEC study, RFQ/3- 7241/91/NL/ BI.

Fomferra, N. And C. Brockmann. The ENVISAT MERIS and AATSR toolbox, 2005. MERIS (A)ATSR Workshop 2005, 597, 13

Gomez-Chova et al., 2010: MERIS/AATSR Synergy Algorithms for Cloud Screening, Aerosol Retrieval, and Atmospheric Correction, Cloud Screening ATBD

Henken, C. C., R. Lindstrot, F. Filipitsch, A. Walther, R. Preusker, and J. Fischer, 2013: FAME-C: Retrieval of cloud otppressure with vertically inhomogeneous cloud profiles. AIP Conference Proceedings, 1531, 412-415

Hollstein, A., J. Fischer, C. Carbajal Henken, and R. Preusker, 2014: Bayesian cloud detection for MERIS, AATSR, and their combination. Atmos. Meas. Tech. Discuss., 7, 11045–11085

Hollstein, A., J. Fischer, 2012: Radiative transfer solutions for coupled atmosphere ocean systems using the matrix operator technique. *Journal of Quantitiave Spectroscopy and Radiative Transfer*, 113(7), 536-548

Hansen, J.E., 1971: Multiple scattering of polarized light in planetary atmospheres. Part I. The doubling method. *J. Atmos. Sci.*, **28**, 120-125

Henken, C. K., R. Lindstrot, F. Fillipitsch, A. Walther, R. Preusker and J. Fischer, 2013 : Retrieval of cloud top pressure with vertically inhomogeneous cloud profiles. In AIP Conference proceedings, 1531, 412

King, M. D., 1987 Determination of scaled optical thickness of clouds from reflected solar radiation measurements. *J. Atmos Sci.*, **44,** 129-144

Lindstrot, R., R. Preusker, T. Ruhtz, B. Heese, M. Wiegner, C. Lindemann, and J. Fischer, 2006: Validation of MERIS Cloud-Top Pressure Using Airborne Lidar Measurements. *J. Appl. Meteor. Climatol.,* **45**, 1612–1621.

Lindstrot, R, Preusker, R. and Fischer, J., 2010: The empirical correction of stray light in the MERIS oxygen A band channel, *J. Atmos. Oceanic Technol.,* **27 (7)**, *1185-1194.*

Merheim-Kealy, P., J. P. Huot, and S. Delwart, 1999: The MERIS ground segment. Int. J. Remote Sens., **20**, 1703–1712.

Nakajima, T., M. D. King, 1988: Cloud optical parameters as derived from multispectral cloud radiometer. Vale, FIRE Science Experiment Team

Nakajima, T., M. D. King, 1990: Determination of the optical thickness and effective radius of clouds from reflected solar radiation measurements. Part 1: Theroy. J. Atmos. Sci., **47**, 1878-1893

Ohring, G. and S. Adler, 1978 Some experiments with a zonally averaged climate model, J. *Atmos. Sci.*, **35**, 186-205

Pavolonis, M. J. and A. K. Heidinger, 2004: Daytime cloud overlap detection from AVHRR and VIIRS, J. Appl. Meteorol., 43, 762-778.

Pavolonis, M. J., A. K. Heidinger, and T. Uttal, 2005: Daytime global cloud typing from AVHRR and VIIRS: Algorithm description, validation, and comparison, J. Appl. Meteorol., 44, 804-826.

Preusker, R., and R. Lindstrot, 2009: Remote Sensing of Cloud-Top Pressure Using Moderately Resolved Measurements within the Oxygen A Band—A Sensitivity Study. *J. Appl. Meteor. Climatol.*, **48**, 1562–1574.

Pruppacher, H. R. 1980 Microstructure of atmospheric clouds and precipitation. *Clouds: Their Formation, Optical Properties adn Effects*, P. Hobbs and A. Deepack, Eds. 93-185

Ramanathan, V., R. D. Cess, E. F. Harrison, P. Minnis, B. R. Barkstrom, E. Ahmad, D. Hartmann, 1989 Cloud radiative forcing and climate: Results from the Earth Radiation Budget Experiment. *Science*, **243**, 57-63

Rodgers, C., 2000: Inverse Methods for Atmospheric Sounding: Theory and Practice. World Scientific, London.

Rothman, L. S., D. Jacquemart, A. Barbe, D. Chris Benner, M. Birk, L. R. Brown, M. R. Carleer, C. Chackerian, K. Chance, L. H. Coudert, V. Dana, V. M. Devi, J. M. Flaud, R. R. Gamache, A. Goldman, J.-M. Hartmann, K. W. Jucks, A. G. Maki, J.-Y. Mandin, S. T. Massie, J. Orphal, A. Perrin, C. P. Rinsland, M. A. H. Smith, J. Tennyson, R. N. Tolchenov, R. A. Toth, J. Vander Auwera, P. Varanasi, and G.Wagner, 2005: The HITRAN 2004 molecular spectroscopic database. J. Quant. Spectrosc. Radiat. Transfer, **96**, 139–204.

Walther et al., 2010: Daytime Cloud Optical and Microphysical Properties, ATBD

Wang, P., P. Stammes, R. van der A, G. Pinardi, and M. van Roozendael, 2008: FRESCO+: an improved O2 A-band cloud retrieval algorithm for tropospheric trace gas retrievals. Atmospheric Chemistry and Physics, **8**, 6565–6576.

Wiscombe, W. J., 1980 Improved Mie scattering algorithm, *Appl. Opt.*, **19**, 15505-1515

Wu, M.-L. C., 1985 Remote Sensing of Cloud-Top Pressure Using Reflected Solar Radiation in the Oxygen A-Band, *J. Appl. Met.*, **24**, 549-546

Yamamoto G., D. Q. Wark, 1961 Discussion of the Letter by R. A. Hanel, Determination of Cloud Altitude from a Satellite´. *J. Geophy. Res*, **66**, 3596

8 Glossary

AATSR	Advanced Along Track Scanning Radiometer
AMSR	Advanced Microwave Scanning Radiometer
ARM	Atmospheric Radiation Measurement (Program)
ATBD	Algorithm Theoretical Basis Document
CGT	Cloud Geometrical Thickness
CLA	Cloud Albedo
CALIOP	Cloud and Aerosol Lidar with Orthogonal Polarization
COD	Cloud Optical Depth
CoG	Centre of Gravity
CPH	Cloud Phase
CPR	Cloud Profiling Radar
CTH	Cloud Top Height
CTP	Cloud Top Pressure
CTT	Cloud Top Temperature
CWP	Cloud Water Path
DCHP	Daytime Cloud Height Properties
DCOMP	Daytime Cloud Optical and Microphysical Properties
ECMWF	European Centre for Medium Range Weather Forecast
FAME-C	FUB AATSR-MERIS Cloud Retrieval
IWP	Ice Water Path
IR	Infrared
ISCCP	International Satellite Cloud Climatology Project

K	Kelvin
LWP	Liquid Water Path
MERIS	Medium Resolution Imaging Spectrometer
MFRSR	Multifilter Rotating Shadowband Radiometer
MODIS	Moderate Resolution Imaging Spectroradiometer
MWR	Microwave Radiometer
NIR	Near Infrared
NWP	Numerical Weather Prediction
OE	Optimal Estimation
REF	Effective Radius
RMSE	Root Mean Square Error
RTM	Radiative Transfer Model
RTTOV	Radiative Transfer for TOVS
SACURA	Semi-Analytical CloUd Retrieval Algorithm
SST	Sea Surface temperature
TOA	Top of Atmosphere
TOC	Top of Cloud
VIS	Visible
WACR	W-band ARM Cloud Radar